

Molecular and Structural Analysis of Viscoelastic Properties

Rebecca D. Yapp, Sureshkumar Kalyanam, and Michael F. Insana

Department of Bioengineering, University of Illinois at Urbana-Champaign
Beckman Institute for Advanced Science and Technology
405 North Mathews Avenue, Urbana, IL 61801, USA

ABSTRACT

Elasticity imaging is emerging as an important tool for breast cancer detection and monitoring of treatment. Viscoelastic contrast in lesions is generated by disease specific processes that modify the molecular structure of connective tissues. We showed previously that gelatin hydrogels exhibit mechanical behavior similar to native collagen found in breast tissue and therefore are suitable as phantoms for elasticity imaging. This paper summarizes our studies of the viscoelastic properties of hydro-polymers to discover the molecular sources of elasticity image contrast.

Keywords: breast cancer, polymer mechanics, ultrasound

1. INTRODUCTION

Elasticity imaging provides spatial maps of mechanical strain that depend on the material properties of the tissue, the geometry of the medium, boundary conditions, and the nature of the applied stress stimulus. Ultrasound is used to image displacements over time from which strain is calculated. If we apply a sudden compressive force to the tissue and hold it constant while measuring strain, we can image time-varying viscoelastic properties in addition to elastic strain, and thereby increase the diagnostic feature space.

Preliminary clinical trials show that elastic strain is a diagnostic feature for benign-malignant discrimination of palpable tumors, and that images of viscoelastic features add discriminability that extends to nonpalpable lesions.¹

In order to accurately detect a harmful lesion, an understanding of the physical properties of the tissue is necessary. Breast tissue mechanically behaves as a viscoelastic polymer. The response a viscoelastic material exhibits is based upon its structural components. In the case of the connective tissue of breast stroma, the primary structural components of the extracellular matrix are collagen fibers surrounded by fluid. Hydrophilic proteoglycan molecules attach to the collagen fibers resulting in structured water surrounding the collagen matrix(**Need source**). The collagen fibers form covalently bonded cross-links among and within themselves. These bonds are difficult to break and thus provide structural rigidity to the network and can be mechanically detected by its purely elastic response. Weaker bonds such as hydrogen bonds are also found throughout the network and are easily broken and reformed at characteristic rates in the presence of an applied stress. This delayed reaction provides the viscoelastic response.

Malignant lesions exhibit certain biochemical characteristics that may help distinguish them from a benign tumor if these characteristics motivate mechanical variations. For instance, malignant tumors are generally stiffer than the background they reside in due to edema, cellular hyperplasia, and an increased collagen concentration. But softer tumors can also occur depending upon the tumors microenvironment. It is known that the extracellular pH of a tumor is acidic due to a reduced buffering capacity by the interstitial fluid of the tumor, poor perfusion, and increased lactic acid secretion. This acidic extracellular pH has consequences such as increased in vivo metastasis, invasion, and mutation.² It has previously been demonstrated that elasticity imaging is sensitive to pH changes.³ The goal of this study is determine imaging parameters for detecting localized pH changes.

Further author information: (Send correspondence to R.D.Y.)
E-mail: ryapp2@uiuc.edu

A model tissue phantom is needed to conduct these studies. Gelatin hydrogels behave mechanically similar to connective tissue and therefore provide a good model for analysis (**which paper says this?**). While lacking in the proteoglycan component, structured water is still present within the matrix. The types of water in gelatin hydrogels have been divided into four classes: (i) water bound by high energy sorption centers, (ii) monomolecular layer structural water, (iii) polymolecular layer structural water, and (iv) free unbound water.⁴ These hydrogels fit into a viscoelastic polymer class described as *very lightly cross-linked amorphous polymers*. This class exhibits a bimodal distribution of elements evident in the loss modulus. The two processes have been described as (i) relative motion of chain segments and (ii) configurational rearrangements of segments.⁵ Based upon recent studies on similar phantoms, it has been proposed that there are two dominant mechanisms present, the first being a fast response due to fluid movement, and the second being longer due to matrix relaxation.⁶

The approach to this study is to first use mechanical testing techniques to analyze how pH changes effect a homogenous hydrogel phantom. Second, mechanical testing experiments are modeled using Finite Element Analysis (FEA) to provide further insight into what material properties effect the various observed responses. Finally, heterogenous phantoms with localized pH changes will be tested using elasticity imaging. Molecular and structural knowledge gained from the first two approaches will assist in the prediction and analysis of imaging parameters.

2. METHODS

There are three approaches taken to develop a baseline mechanistic understanding of our gelatin models when subjected to pH changes. These include two experimental approaches: unconfined compression and confined compression; as well as FEA simulations of the confined experiments. Elasticity imaging experiments take the basic form of the unconfined compression test, thus experimental parameters developed for these tests will parallel those of the unconfined case. This section starts with a brief explanation of the constitutive equations used to model the experimental data as well as the theory behind the testing conditions. Followed by, detailed descriptions of the experimental methods and finite element analysis.

2.1. Constitutive Equations

A more detailed description of the constitutive equations used in this study are described in detail elsewhere and have been demonstrated to be good models for experiments on hydrogels of this type.^{6,7} The unconfined compression and elasticity imaging experiments are creep experiments in which a step uniaxial compressive stress, $\sigma_a(t)u(t)$ is applied as the strain is measured as a function of time under free slip boundary conditions, as illustrated in Figure 1a,c. These creep experiments can be modeled using a discrete generalized Voigt model,

$$\varepsilon(t) = \varepsilon_0 + \sum_{k=1}^K \varepsilon_k (1 - \exp(-\frac{t}{T_k})) + \frac{1}{\eta_0} t \quad (1)$$

Where $\varepsilon(t)$ is the strain, ε_0 is the initial elastic response, ε_k are the individual strain amplitude components with time constants T_k for each discrete element, and η_0 is the viscosity term. The initial elastic response is the strain measured immediately after the stress is applied and is directly proportional to the compressive compliance (or inversely proportional to the elastic modulus). Therefore, the time varying compression compliance function can be written as, $D(t) = \varepsilon(t)/\sigma_a$. The next K components represent the viscoelastic response of the material. The final term is a purely viscous component in the polymer that varies linearly with time and represents unbound fluids.

It is desirable to analyze the loss compliance of the creep response because it provides further insight into the viscoelastic response. According to Tschogel⁸ the loss compliance is related to the time domain model as,

$$D(\omega) = -\Im \frac{s\bar{\varepsilon}(s)}{\sigma_a} \Big|_{s=i\omega} = \sum_{k=1}^K \frac{(\varepsilon_k/\sigma_a)\omega T_k}{1 + \omega^2 T_k^2} \quad (2)$$

Where $\bar{\varepsilon}(s)$ is the Laplace transform of the time domain strain data. In the material properties sense, the loss modulus represents energy dissipated (viscoelastic components, and viscous component) as opposed to stored

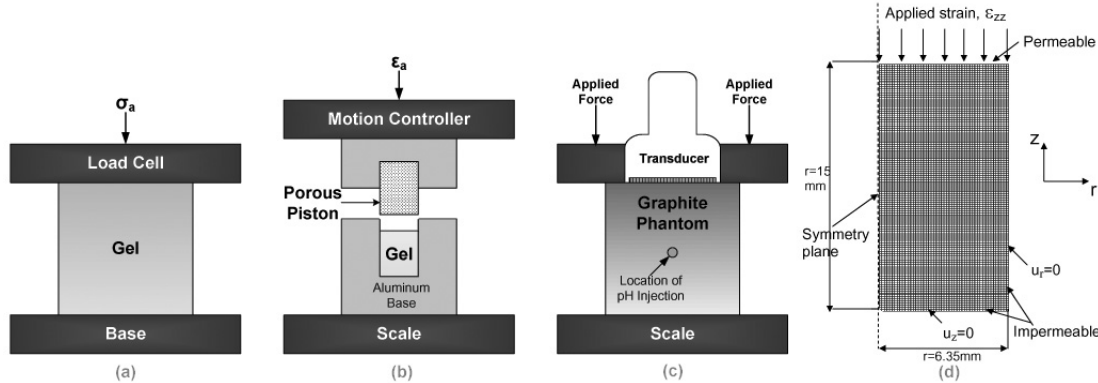


Figure 1. This figure displays schematics of the three experimental methods and FEA model. Method (a) is unconfined compression, method (b) is confined compression, method (c) is elasticity imaging, and method (d) is the FEA model of confined compression.

energy (elastic components). It should be noted that last equality in equ (2) is only valid if the linear viscous flow term is removed prior to taking the Laplace transform of the time domain data, else the loss compliance function will be offset by the constant value $1/\eta_0$. It is also important to point out that the maxima of the loss compliance occur at $\omega = 1/T_k$. Thus, frequency domain analysis can be useful in determining an appropriate number of discrete viscoelastic elements to include in the model.

The parameters described in equ (1) are all potential imaging parameters. Each providing insight into the intrinsic structural and molecular properties of a material. The time domain strain data of the unconfined and imaging experiments are fit to a discrete Voigt model as described elsewhere^{6,7} using the Matlab function LSQCURVEFIT. Once again, the linear viscous term must be subtracted in order for the curve fitting to converge upon a good model fit (consequently, the estimation of η_0 is performed independently of the other parameters). The strain data is obtained differently for the two techniques. For the unconfined experiments, the change in the entire gels height is tracked. For the imaging experiments, the strain is tracked as a function of space and time in a 2-D imaging plane.

Confined stress relaxation experiments differ from unconfined creep experiments in terms of the applied stimulus and boundary conditions. In a confined test, all boundaries of the sample are confined except for one as illustrated in Figure 1b. For this study, the unbound direction is normal to the surface of the gel. The stimulus is a constant step strain $\epsilon_a u(t)$ applied by a porous piston through which energy can dissipate. Similar to creep experiments, time domain confined stress relaxation data can be modeled by a discrete Maxwell model described by its wave modulus $M(t)$ and corresponding loss modulus $M''(\omega)$.⁸

$$M(t) = \frac{\sigma(t)}{\epsilon_a} = M_0 + \sum_{k=1}^K M_k \exp(-t/\tau_k) \quad (3)$$

$$M''(\omega) = \Im s \overline{M}(s) |_{s=i\omega} \quad (4)$$

Because of the boundary condition differences between the confined and unconfined experiments, curve fitting is not performed on confined data because the model parameters are not interchangeable. However, the spectral response is analyzed because it provides another angle of insight into the types of contributing material response components. Confined stress relaxation data provides a means of delineating the mechanical responses of a material because of the boundary conditions. With this geometry, the gel may only relax after losing energy through the porous piston, this behavior creates a time delay between responses and may be separable in the loss spectrum.

2.2. Gelatin Phantom

All phantoms are constructed using Type B 250 bloom strength gelatin provided by Rousselot. This specific gelatin was chosen for its stability around its isoelectric and isoionic point. This stability results in easy shifts

in pH. A typical phantom includes 8% w/w gelatin, 91.9% w/w deionized water and 0.01% w/w formaldehyde. Under these conditions the 'neutral' pH of the hydrogel ranges between 5.5 to 5.7. Addition of approximately 1.5% w/w 1N HCl will shift the pH down one unit to 4.6 and the addition of 0.6% w/w 1N NaOH shifts the pH up one unit to 6.6. More hydrogen ions are needed to shift the pH down to 4.6 than hydroxyl ions to shift to pH 6.6 because of the nature of Type B gels titration curves; an example titration curve for alkali treated gelatins is given by Veis⁹ which agrees with this finding. The combination of gelatin and water is heated in a water bath to 55-65°C for 1 hour and periodically stirred. This process heats the gel above its melting point of 35°C and allows a clarified mixture to form. After heating, formaldehyde and necessary additions of HCl or NaOH are added. The gel is then allowed to cool to room temperature (21-22°C). The total polymerization time (t_p) is considered to be the time from which the gel is allowed to start cooling until the time the sample is tested. There are slight variations in the sample preparation among the types of experiments, including the addition of n-propanol (9.1%w/w) and graphite (3.4% w/w). Graphite is used for the ultrasonic imaging phantoms to provide a scattering media and a higher attenuation coefficient. The n-propanol was only used in the confined tests. Regardless of these variations between experiments, the mechanical differences observed should be low enough to neglect. According to Hall et al.¹⁰ graphite produces a small effect on gel stiffness giving an elastic modulus difference on the order of 1kPa between a sample with and without graphite at 5.5%w/w concentration. When n-propanol is not used, its concentration is replaced by additional water of an equivalent percentage. Since the purpose of all the experiments is to determine the mechanical effects of pH changes, these slight variations will not effect the overall data trends. For future experiments more care will be taken to ensure the consistency of sample preparation throughout methods. The specific experimental techniques will be described in each of the corresponding sections.

2.3. Unconfined Compression

Unconfined compression tests are performed on cylindrical gelatin phantoms 44.45mm height and diameter. The procedure for cooking these gels is precisely as stated in section 2.2. When the gel is removed from the heat it is allowed to cool to 50°C before formaldehyde and necessary HCl or NaOH are added. The gel is then cooled to 45°C before being poured into molds. The phantom mold is constructed of cylindrical acrylic tubing (50.8mm O.D., 44.45mm I.D., 44.45mm height) and 2 flat acrylic plates (50mm x 50mm x 6.35mm). The two plates are clamped to the open cylinder ends to make an air tight seal. Mold release (Pol-Ease 2300 by Polytek) coats the inside of the mold to prevent the gel from adhering to the plastic. The gel is poured into the cylinder through a syringe attached its side. The gel is allowed to congeal at room temperature for the next 41 hours. After 41 hours the gel (still in its mold) is placed into a 2°C refrigerator for 30 minutes; doing so allows the gel to easily release from the mold. Immediately after the gel is removed from its mold, it is placed in an airtight container for 3 hours before testing. This is a sufficient amount of time to allow the gel to equilibrate back to 21°C.

All unconfined experiments are performed using a TA.XT Plus from Texture Technologies Corp. As simply illustrated in Figure 1a, σ_a is applied by a 3 cm diameter aluminum compressive plate. The sample is unbound in the lateral directions and the top and base of the sample are coated with oil to simulate the free slip boundary conditions. The TA.XT Plus has a 1kg (+/- 0.01g) load cell attached to the compression plate that senses the applied stress and provides feedback to the system to adjust the height of the probe as necessary. This displacement adjustment over time corresponds to the strain response of the gel.

To determine the creep testing parameters, stress-strain curves are obtained by first applying a 30g pre-load ($\sim 5\%$ strain) followed by an additional 10% strain at a frequency of 0.04Hz on neutral gelatin phantoms (pH 5.6). These experiments determined pre-conditioning parameters as well as the experimental conditions to assume linear viscoelastic behavior (the linear regime). Stress-strain data suggests that the neutral gelatin stabilizes after about 35 cycles, and the loading curve is approximately linear over the range of 10% strain (engineering strain) as displayed in Figure 2. By taking the slope of the loading portion of the stress-strain curve of the 40th cycle the elastic modulus can be estimated. For 3 samples of neutral pH gelatin, the elastic modulus was estimated to be 11.3kPa with a standard deviation of 0.1kPa. Based upon this data the creep testing procedure will be to (1) precondition the sample by applying a 30g pre-load and cycle through 0-10% engineering strain at 0.04Hz for 40 cycles, and (2) initiate the creep test immediately following the preconditioning. The applied stress is chosen to be 720Pa because it is within the linear regime of the gel and it is within the range of the applied stress for

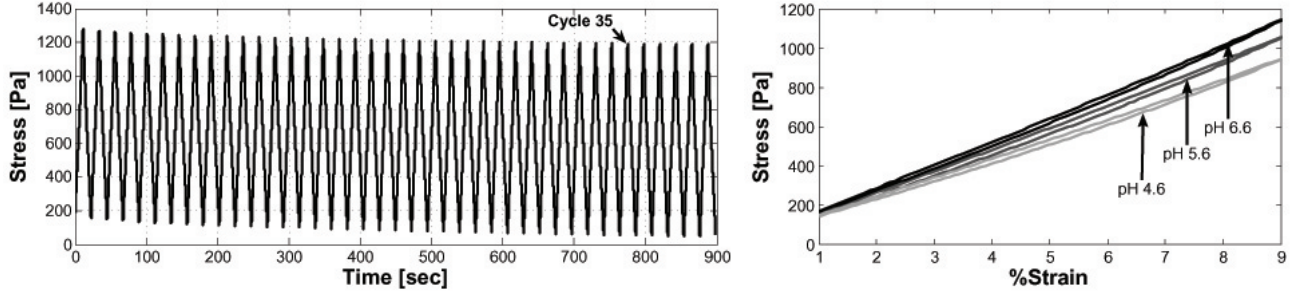


Figure 2. The stress vs. time plot is displayed for a neutral pH sample. The gel is loaded and unloaded at a frequency of 0.04Hz for 40 cycles. Stability is achieved at approximately cycle 35. The figure on the right displays the stress-strain curves of the 40th cycle for each of the 3 pH values displayed.

unconfined imaging experiments (see Section 2.6). The σ_a will be applied in 1.5 seconds (an approximate unit step stress) and held for 30 minutes.

2.4. Confined Compression

In confined compression, a cylindrical gelatin sample (height = 15mm, diameter = 12.7mm) is bounded by an aluminum confining chamber as depicted in Figure 1b, in order to ensure that the elastic modulus of the chamber (70GPa) is much greater than that of the sample (11kPa). A porous polyethylene piston (35 μ m pore size), with a diameter 0.25mm less than that of the base which encompasses the gel, strains the gel 2%. This strain is applied using a motion controller (Galil) in 1 second (to simulate a unit step strain) and is maintained for 30 minutes while the stress is measured as a function of time using a digital scale (Denver Instruments Model TR-4102).

The hydrogel used in these experiments is composed of 82.8% w/w deionized water, 9.1% w/w n-propanol, 8% gelatin, and 0.1% w/w formaldehyde. The solution of water, propanol and gel is cooked for one hour followed by the addition of formaldehyde and necessary HCl or NaOH as stated in section 2.2. The hot gel solution is poured into the aluminum base and care is taken to remove any air bubbles. A flat cap coated with mold release is placed on top of the gel surface to create a flat top surface. The base and cap apparatus create a mold for the gel, for experimentation purposes the cap is removed and the gel is left in the base for testing. The t_p for these samples is 48 hours.

2.5. Finite Element Analysis

Uniaxial confined compression tests performed to observe the stress-relaxation behavior of gelatin were simulated using the commercial ABAQUS FEA software. The biphasic poroelastic and poroviscoelastic theory has been widely used in the finite element modeling of cartilage by several researchers.^{11–15} In the present modeling approach, gelatin is assumed to be a biphasic material consisting of denatured collagen network (elastic porous matrix) and fluid that fills the rest of the extra-cellular matrix (ECM) space interstitial fluid). The gelatin material is assumed to be a poroelastic material and the widely accepted and used consolidation theory is used in the FEA. The material parameters used in the FEA are the Young’s modulus and Poisson’s ratio of the drained porous matrix (E_m and ν_m), permeability (κ) and the initial void ratio (e_0), i.e ratio of fluid content to solid matrix. We use the material model in ABAQUS and assume that the poroelastic material has all the pores (voids) to be saturated with fluid. For example, a 6% gelatin specimen has a fluid content of 94% by net weight during preparation and the fluid content is found to be close to 94% from desiccation experiments performed on gelatin specimens of various sizes. The Young’s modulus and Poisson’s ratio were obtained from the experimental testing of gelatin phantoms performed by Sridhar *et al.*⁶ An initial estimate of the permeability was obtained by performing a FEA of the compression experiment conducted to measure the change in Poisson’s ratio under an applied step strain⁶ and the initial estimate of permeability was chosen based on the prediction of the experimentally measured lateral strain. The material parameters used in the FEA were: $E_m = 10.83kPa$, $\nu_m = 0.47$, $e_0 = 15$, and κ varied from 5×10^{-8} to 7×10^{-6} m/s.

In the confined experiments conducted, the gelatin specimen is placed in a holder and the load is applied by a porous piston. Since the gelatin specimen is cylindrical we perform an axisymmetric analysis using CAX8P 8-node axisymmetric finite elements which include pore pressure. The displacement field is obtained by interpolation of all 8 nodes and is quadratic and the pore pressure is obtained by interpolation of the 4 corner nodes and is hence bilinear in variation within the finite element. The finite element model, shown in Fig. 1 represents one half of the specimen (radius, $R=6.35\text{mm}$, height, $H=15\text{mm}$) due to axisymmetry and composes of 6000 elements and 18341 nodes. A frictionless boundary condition is assumed between the metallic holder and the gelatin specimen, such that the gelatin slips freely during deformation in the axial (z direction) when the compressive load is applied. The boundary conditions are shown in Figure 1d. The axis $r=0$ and $r=R$ has no fluid flow (impermeable) and no displacement in the radial direction, $u_r = 0$. The bottom of the specimen, $z=0$ has no vertical displacement, $u_z = 0$ and has an impermeable boundary condition. The top of the specimen has vertical displacements specified corresponding to the strain applied in the experiments and has a permeable boundary condition since the fluid exudes into the porous piston through this gelatin surface.

2.6. Ultrasonic Elasticity Imaging

The purpose in this elasticity imaging study is to detect contrast due to pH changes in a heterogenous phantom. This is accomplished by creating an inclusion in the center of the phantom that is allowed to polymerize in the presence of an acid or a base. The goal of the inclusion is to introduce a localized pH change to the gelatin before it has completely polymerized, thus simulating an environment that is representative of biochemical processes in the body. The gelatin imaging phantoms are constructed using a modification of a procedure previously described.¹⁰ As described in section 2.2, water and gelatin are heated for one hour, then allowed to cool at room temperature until the internal temperature reaches 50°C . At this point, the formaldehyde is added. The gel then continues to cool to 45°C after which 3.35% w/w graphite is mixed into the gel. The gel is covered and periodically mixed to prevent the graphite from settling until the temperature reaches $38\text{-}40^\circ\text{C}$. Then the gel is placed in a vacuum chamber to degas the solution and then poured into a cubic phantom case and rotated for approximately 2.5 hours to guarantee a homogenous mixture. The phantom case is a 5cm cubic case. The interior is coated with mold release and a piece of PE 50 tubing is inserted and sealed with silicone through two exit holes centered on parallel sides of the case. The 2.5 hour rotation is the time it takes for the gel to form an interwoven polymer network that still is free to flow as a viscous fluid; this is the time at which the pH injection will take place. Injection at this time will cause the injected fluid to interact with the viscous gelatin before it has completely polymerized. The injection procedure is as follows: the silicone seal around the exterior of the PE 50 tubing is loosened such that the tubing may be pulled through the phantom while the phantom is still congealing in the case. A 3mL syringe connected to a syringe pump with a 27 gauge needle is inserted into the tubing. The syringe pump allows the injection fluid to flow through the tubing at a flow rate of $0.5\text{mL}/\text{min}$. As the fluid is flowing through the tubing, the tubing is simultaneously pulled through the phantom leaving a channel of fluid in its path. Once the injection is complete, the case exit holes are sealed with hot glue and the phantom continues to congeal until $t_p = 48$ hours. Three phantoms are constructed: an acidic injection of 1N HCl, a neutral injection of pH 5.6, and a basic injection of 1N NaOH.

Strain imaging experiments are performed on these injection phantoms using an apparatus as depicted in Figure 1c. This experimental technique is based upon previous work by Sridhar *et al.*⁷ The phantom is coated in oil to simulate free-slip boundary conditions and minimize desiccation. A flat plate that holds the ultrasound transducer is attached to a motion controller. The motion controller is programmed to ramp up (1.5 seconds) to apply a constant uniaxial stress for 700 seconds. The stress is applied perpendicular to the surface of the sample which is placed on a digital scale. The scale provides feedback to the motion controller of the measured stress in order to maintain the appropriate displacement (within $0.1\mu\text{m}$) to achieve a constant stress. The displacement is recorded from the motion controller at approximately 8 samples per second. In imaging phantoms, strain is estimated over a 2-D image plane and the applied stress refers to the stress applied over the entire phantom; since imaging phantoms are heterogenous is not possible to extract the applied stress of a particular location. However, in relation to the unconfined experiments, the applied stress to the entire phantom based upon its geometry ranges between 700-1200 Pa (within the linear regime of these particular gels).

Strain images are generated by a constant reference multi-resolution cross correlation technique¹⁶ using RF echo data acquired by Siemens Sonoline Antares system and a VF10-5 linear array transducer transmitting at

8MHz. A 100g pre-load is applied to ensure good acoustic contact between the phantom and transducer. The ultrasound research interface (URI) option of Antares allows use of an external waveform generator (Wavetek 30Ms/s Universal Waveform Generator Model 39) attached to the ECG input to trigger data acquisition. Due to a limited memory capacity, the number of frames per acquisition is limited. The RF data is acquired at 4 frames per second for the first 80 seconds and then at 2 frames per second for the final 620 seconds. The first acquisition sequence is faster in order to capture the initial elastic response and any short duration time constant response.

Antares assumes that the speed of sound of the medium it is propagating through is 1540m/s, the average speed of sound in mammalian soft tissue. Attenuation measurements were performed on a homogenous (pH 5.6) imaging phantom to determine the attenuation coefficient and the compressional sound velocity using a narrowband substitution technique(**Need E Madsen Ref**). A calibration was performed using castor oil for $\alpha(f) = 0.09f^{5/3}$ with results within 15% of the expected value according to Dunn(**Need Reference of Floyd Dunn's Chapter). The phantoms average speed of sound across frequencies is approximately 1515 m/s and the attenuation coefficient is $\alpha_0 = 0.3 \text{ dB cm}^{-1}\text{MHz}^{-1}$. Given that the speed of sound mismatch is about 1.5% error, image distortion will not cause a significant error.

3. RESULTS

3.1. Unconfined Compression

By testing homogenous phantoms in unconfined compression, we are able to obtain material information specific to pH changes. This knowledge is useful in the sense that it can be used to explain and predict what will happen in a heterogenous imaging phantom. For each of the three pH levels tested (4.6, 5.6, 6.6) three creep experiments are performed. Due to a good mechanical testing system and systematic sample preparation, experimental results are reproducible among independent samples. A sample that strains more in a creep test is considered to be a softer sample. It is evident from the amplitude differences displayed in Figure 3a that the stiffness increases with pH. As mentioned in section 2.1, it is necessary to remove the linear viscous flow from creep data in order to generate the loss modulus without amplitude offsets and successfully fit the data to a Voigt model. Figure 3b demonstrates a creep curve as obtained experimentally ($\varepsilon(t)$) in comparison to the same data after the linear term has been estimated and removed ($\varepsilon(t) - t/\eta_0$). The linear term is estimated by analysis of the derivative of the acquired creep data, using the idea that the derivative of equ (1) would be a constant value in locations where the linear term contribution was dominant. By estimating a value over such a range would give the slope of the linear term ($1/\eta_0$). If the modified data has a negative slope present, the subtracted term is adjusted accordingly. After subtraction, the corresponding loss modulus can be generated as seen in Figure 3c and the data can be fit to K exponential component Voigt models. Because of the expected bimodal behavior of the gels, the focus will be on bi-exponential models (K=2). The curve fitting parameters among all of these experiments were extracted and compared as a function of pH as depicted in Figure 4. It is clear from these results that the amplitudes (corresponding to the elastic properties) provide contrast and also demonstrate the trend that stiffness increases with pH. The viscosity term (η_0) also increases with pH, indicated that a higher pH has a smaller free fluid flow contribution. On the other hand, the time constant contrast does not show any significant differences within experimental error. It is difficult to obtain any significant information regarding model order of the unconfined tests from spectral analysis since the geometry of this test is likely to allow both fluid and matrix relaxation to start occurring immediately at the onset of the applied stress. The loss spectra as displayed in Figure 3c appears to be one broad distribution of processes.

3.2. Confined Compression and FEA

Confined compression is a difficult task to perform experimentally, because it is extremely sensitive to any experimental uncertainties. Consequently, representative experimental parameters are not estimated from this data. However, it is possible to distinguish trends among independent experiments with samples of varying pH. In agreement with unconfined tests, the confined data also indicates an increase in stiffness with pH as seen in Figure 5a (In stress-relaxation experiments and higher stress refers to a stiffer sample). Since the benefit of the confined test is the ability to delineate processes, spectral analysis is used as the primary tool for interpretation. As illustrated in Figure 5b, the spectral response indicates two peaks, one high-frequency peak occurring around 6

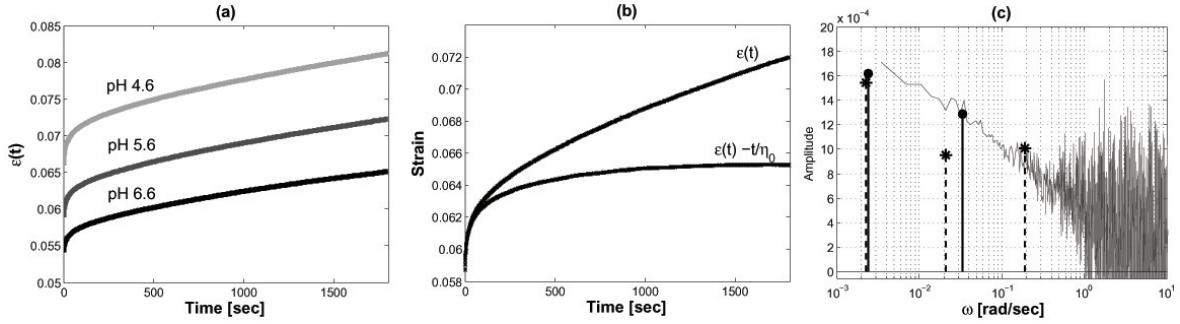


Figure 3. Strain data obtained from unconfined creep tests. (a) Creep curve for 3 pH levels, (b) example of creep curve after linear viscosity term is removed, (c) corresponding loss spectra of data in (b) displaying the location of amplitude scaled time constants from curve fitting a bi-exponential (—●) and tri-exponential (- -*) Voigt models.

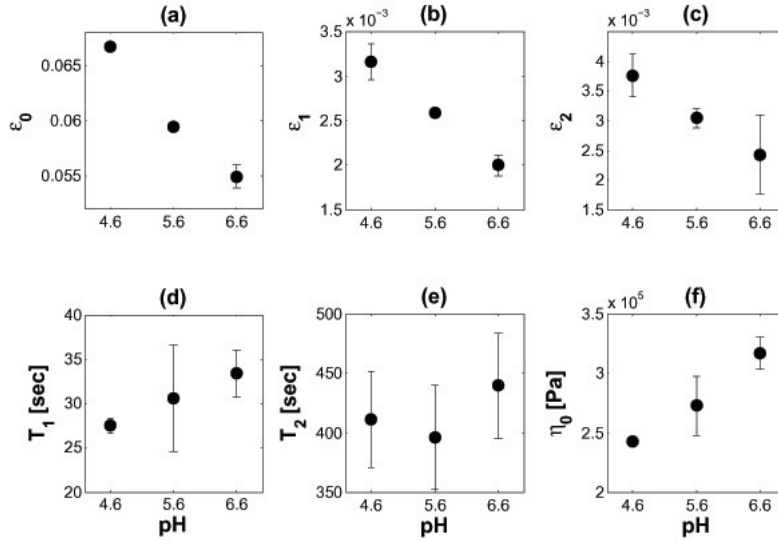


Figure 4. A bi-exponential Voigt model was fit to each of the three sets of unconfined creep data. The model parameters mean values are displayed with corresponding error bars of \pm one standard deviation from the mean.

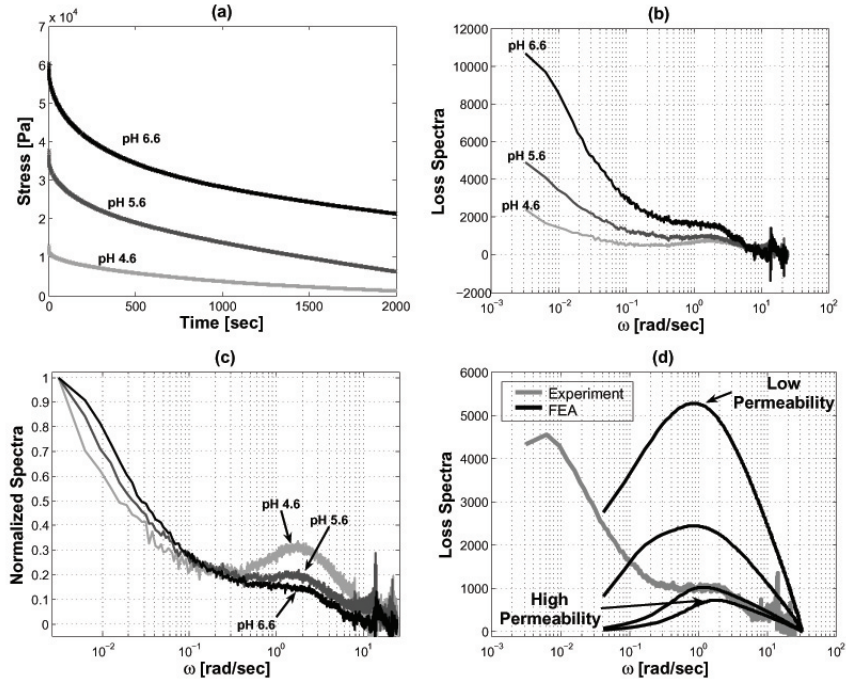


Figure 5. Results from confined experiments and poroelastic FEA simulations. (a). Example of confined stress relaxation data at different pH values. (b). Corresponding loss spectra of time domain data. (c). Loss Spectra of experimental data normalized to the lowest frequency. (d). Poroelastic FEA simulation displaying the effect of permeability on the high frequency peak.

second and the other low frequency peak occurring around 1000 seconds. Among pH data, the amplitude response evidently changes while the peak locations remain constant. The exudation of the free fluid was envisaged to cause the spectral peak at short times and the spectral peak at longer times is attributed to the response of the matrix and the polymolecular structured water which is not relatively free for movement at low forces. In order to validate our hypothesis, different values of permeability (κ) (represents the ease of movement of the free fluid through the ECM) were assumed in the FEA and the spectral variation was obtained. The spectral analysis of the stress variation obtained from FEA confirmed that the high frequency peak is due to the exudation of the free fluid from the interstitial space and the change in permeability alters the magnitude of the peak as seen in Figure 5d. It can also be inferred that the amplitude differences observed between the pH levels are influenced by the permeability changes such that a higher pH has a lower permeability. By normalizing the spectral data to the low frequency peak, the relative high frequency peak contributions can be further analyzed. As shown in Figure 5c, the relative unbound water contribution is greater for lower pH values.

3.3. Elasticity Imaging

Elasticity imaging was performed on the three injections phantoms. As shown in Figure 6, the standard B-mode image does not show any contrast, however when amplitude based strain images are generated, inclusion contrast is evident. Figure 6 shows the strain images generated from the ε_0 parameter for all three phantoms. The amplitudes have been scaled according to the mean background strain among samples. In all cases there is a central bright spot indicating a softening at the injection location. Both the acidic and neutral phantoms show a localized softening, but the acidic appears to have a broader soft region. On the other hand, the basic phantom shows a stiffening effect around the injection point. The results indicate that there is a localized softening effect from the additional fluid introduced, but as the injection fluid diffuses outward, the polymerization process is altered. This alteration corresponds to a change in mechanical properties in agreement with the mechanical testing experiments.

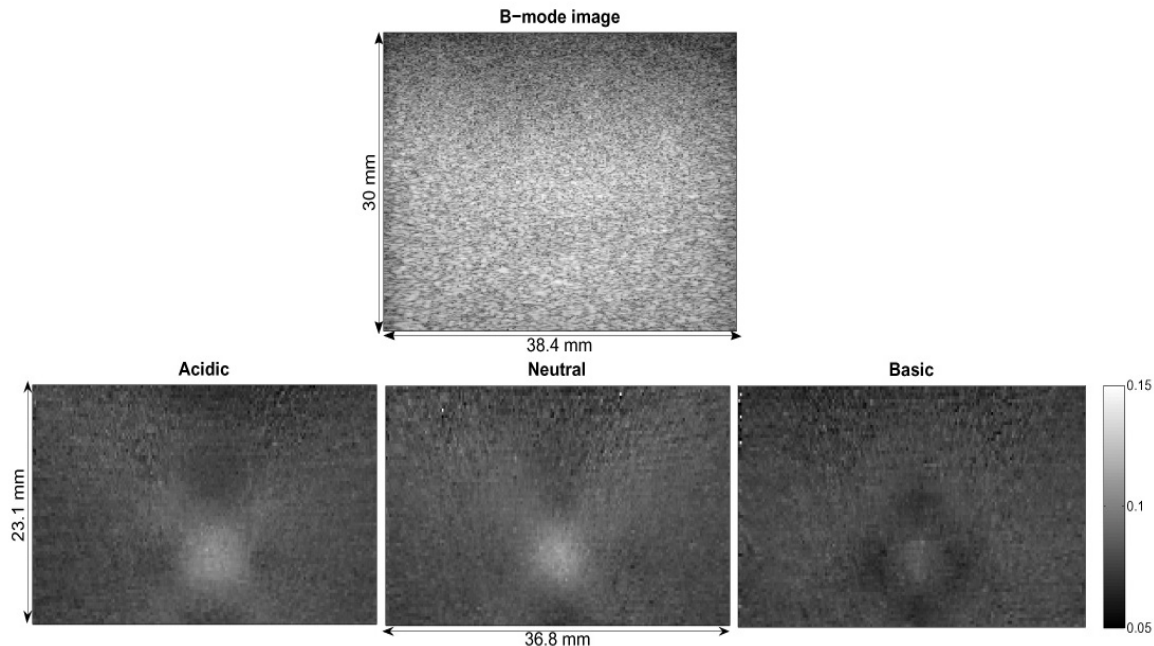


Figure 6. Top: Pre-compression B-mode image of injection phantom. Bottom: Strain images of the three pH injection phantoms for $t_p = 48$ hours.

4. SUMMARY AND CONCLUSION

The mechanical testing results indicate that pH shifts cause distinct amplitude differences but the response time of discrete transient components does not provide means for contrast. As the pH increases, the stiffness increases. The free fluid component which has shown to increase with a lower pH also has potential for providing contrast. Elasticity imaging results of the initial elastic response confirm that amplitude changes can provide contrast. These studies have indicated that an increase in pH provides a more highly structured polymer. Perhaps, the excess of OH^- ions provides more binding sites for water causing an increase in the amount of structural water.

In order to gain a better understanding of the contribution of other components, more work needs to be done. It is not certain that the gels are best represented by a bi-exponential model, a higher order may be more representative. For example, in Figure 3c the location of the amplitude scaled time constants are indicated on the loss spectra plot for both a $K=2$ and 3 model. In both cases, the long time response amplitudes and locations agree, but in the shorter time responses, the $K=3$ model suggests that there may be two contributing components rather than one. Instead of the system being described as a two component model of fluid + matrix, it may be more descriptive to call it a 3 component exponential system of unbound water + mono/polymolecular layered water + matrix entanglements & bound water. A viscoelastic model for both confined and unconfined compression is being developed to be used in FEA to model the matrix phase and will enable the prediction of the low frequency responses. Further analysis and experimentation of elasticity imaging needs to be performed in order to gain a better understanding of how and if viscoelastic properties can be imaged. This study has provided a baseline structural understanding of how pH will change the mechanical properties of this material. The preliminary imaging results show that it is feasible to image localized pH changes.

ACKNOWLEDGMENTS

The authors acknowledge the assistance of Mr. Darren Pocci. Gelatin used in all studies was generously provided by Rousselot. This material is based on work supported by the NCI under award No. CA082497.

REFERENCES

1. M. S. Keralapura, *Imaging viscoelasticity in hydropolymers and breast tissue with ultrasound*, Ph.D. Dissertation, University of California, Davis, 2007.
2. R. J. Gillies, N. Raghunand, M. L. Garcia-Martin, and R. A. Gatenby, “ph imaging,” *IEEE Engineering in Medicine and Biology Magazine* **September/October**, pp. 57–64, 2004.
3. M. Sridhar and et al., “Ultrasonic imaging of biochemical changes in tissues,” *Proc IEEE Ultrasonics Symp.*, pp. 2145–2148, 2004.
4. I. Yakimets and et al., “Mechanical properties with respect to water content of gelatin films in glassy state,” *Polymer* **46**, pp. 12577–12585, 2005.
5. J. D. Ferry, *Viscoelastic Properties of Polymers, 3rd ed.*, John Wiley and Sons, New York, 1980.
6. M. Sridhar, J. Liu, M. F. Insana, and T. A. Krouskop, “Elasticity imaging of polymeric media,” *ASME J. Biomech. Eng.*, (April 2007, in press).
7. M. Sridhar, J. Liu, and M. F. Insana, “Viscoelasticity imaging using ultrasound: Parameters and error analysis,” *Submitted to Physics in Medicine and Biology*, in press.
8. N. W. Tschoegl, *The Phenomenological Theory of Linear Viscoelastic Behavior*, Springer, New York, 1989.
9. A. Veis, *The Macromolecular Chemistry of Gelatin*, Academic Press, New York, 1964.
10. T. J. Hall, M. Bilgen, M. F. Insana, and T. A. Krouskop, “Phantom materials for elastography,” *IEEE Trans. Ultrason. Ferro. Freq. Contrl.* **44**, pp. 1355–1365, 1997.
11. L. P. Li and et al., “Nonlinear analysis of cartilage in unconfined ramp compression using a fibril reinforced poroelastic model,” *Clinical Biomechanics* **14**, pp. 673–682, 1999.
12. J. K. Suh and M. R. DiSilvestro, “Biphasic poroviscoelastic behavior of hydrated biological soft tissue,” *Transactions of the ASME* **66**, pp. 528–535, 1999.
13. M. R. Silvestro and J. K. Suh, “A cross-validation of the biphasic poroviscoelastic model of articular cartilage in unconfined compression, indentation, and confined compression,” *Journal of Biomechanics* **34**, pp. 519–525, 2001.
14. R. K. Korhonen and et al., “Fibril reinforced poroelastic model predicts specifically mechanical behavior of normal, proteoglycan depleted and collagen degraded articular cartilage,” *Journal of Biomechanics* **36**, pp. 1373–1379, 2003.
15. W. Wilson and et al., “Stresses in the local collagen network of articular cartilage: a poroviscoelastic fibril-reinforced finite element study,” *Journal of Biomechanics* **37**, pp. 357–366, 2004.
16. P. Chaturvedi, M. Insana, and T. Hall, “Testing the limitations of 2-D companding for strain imaging using phantoms,” *IEEE Trans. Ultrason. Ferroelec. Freq. Control* **45**, pp. 1022–1031, 1998.